Connectivity of icosahedral network and a dramatically growing static length scale in Cu-Zr binary metallic glasses

Ryan Soklaski, Zohar Nussinov, Zachary Markow, K. F. Kelton, and Li Yang

Phys. Rev. B **87**, 184203 — Published 23 May 2013

DOI: 10.1103/PhysRevB.87.184203

Connectivity of the Icosahedral Network and a Dramatically Growing Static Length Scale in Cu-Zr Binary Metallic Glasses

Ryan Soklaski, Zohar Nussinov, Zachary Markow, K.F. Kelton, and Li Yang
Department of Physics, Washington University in St. Louis, St. Louis, MO 63130, USA

We report on and characterize, via molecular dynamics (MD) studies, the evolution of the structure of $Cu_{50}Zr_{50}$ and $Cu_{64}Zr_{36}$ metallic glasses (MGs) as temperature is varied. Interestingly, a *percolating icosahedral network* appears in the $Cu_{64}Zr_{36}$ system as it is supercooled. This leads us to introduce a static length scale, which grows dramatically as this three dimensional system approaches the glass transition. Amidst interpenetrating connections, non-interpenetrating connections between icosahedra are shown to become prevalent upon supercooling and to greatly enhance the connectivity of the MG's icosahedral network. Additionally, we characterize the chemical compositions of the icosahedral networks and their components. These findings demonstrate the importance of non-interpenetrating connections for facilitating extensive structural networks in Cu-Zr MGs, which in turn drive dynamical slowing in these materials.

I. INTRODUCTION

Understanding the structure-property relationships of metallic glasses (MG) is a pressing matter in the field of material science[1–5]. The culmination of past research reveals that the vast diversity of MG species, and their properties, are rooted in an equally-broad set of structural archetypes[6–8]. Perhaps even more cumbersome is a decades old outstanding problem in the study of glasses-namely explaining the extreme slowing of dynamics in a liquid as it is supercooled towards a glass transition[9–34]. Many theories, such as the theory of random first order transitions[10,11], spin glass approaches[12], and others[16–18] predict the existence of rapidly growing length scales (in particular, a static length scale) to accompany the marked increase of the viscosity of supercooled liquids. In fact, there are rigorous results predicting the appearance of such lengths[33]. While much progress[18–28] has been made in studying the structures of various glass-forming systems, to date, no notable increase in standard static length scales has been observed in most studies.

Cu-Zr is a popular representative of Early Transition Metal-Late Transition Metal MGs; this is, in part, because it has a high glass forming ability (GFA) for a broad range of compositions[35–39]. The binary composition of Cu-Zr reduces the complexity of the possible local atomic structures, making this system ideal for the study of the evolution of the spatial structure of liquids as they are supercooled to form a glass. Recent research efforts demonstrate a structural hierarchy within Cu-Zr MGs that appears to be central to its structure-property relationships[34,41–46]. Strong evidence has been found to suggest that the presence of Cu-centered full icosahedra is uniquely responsible for dynamical slowing during the formation of the Cu-Zr MGs[34,41,42]. Aside from their full and distorted icosahedral Voronoi signatures, the Voronoi polyhedron landscapes of Cu-Zr in the liquid and glass phases resemble one another considerably[47]. The icosahedral clusters often interpenetrate one another, so that five atoms coincide on two icosahedral-shells. These interpenetrating connections of icosahedra (ICOI) exhibit strong spatial correlations[34,47] and produce stable string-like networks of icosahedra[34,46–50]. Extensive ICOI clusters are found to posses a high average elastic rigidity[46] and to enhance more general mechanical properties of Cu-Zr[42] MG.

In light of the importance of icosahedral clusters and ICOI in shaping Cu-Zr MG, it is pressing to consider the roles of non-interpenetrating connections in order to obtain a complete picture of icosahedral networking in this amorphous alloy. To date, the prominence of these connections has only been noted[34]. In this paper, MD simulations are used to study non-interpenetrating connections, and to characterize their effect on the connectivity and composition of icosahedral networks in Cu-Zr MGs, using $Cu_{50}Zr_{50}$ and $Cu_{64}Zr_{36}$ as models. Our analysis reveals that, near the glass transition, a large number of non-interpenetrating connections develop amongst ICOI-structures and significantly enhance the unification of icosahedral networks in these MGs, thus impacting their mechanical properties. Considering the full icosahedral network affords us the rather unique opportunity to identify, in $Cu_{64}Zr_{36}$, *a percolating icosahedral network that threads the entire glassy system, providing a large scale static structure which grows rapidly as the system approaches the glass transition.* We also suggest that the non-interpenetrating connections are particularly influential in MGs like $Cu_{50}Zr_{50}$, which exhibits relatively few ICOI and yet is a good glass former. Moreover, with all of the connection types being included, we reveal that the icosahedral network and the otherwise liquidlike matrix[47] have significantly different chemical compositions. For example, vertex and face-sharing connections preferentially incorporate Zr atoms, increasing the density of the icosahedral network. For both alloys, the icosahedral network is Zr-rich, relative to the overall sytem composition, and is immersed in a Cu-rich liquidlike matrix.

In section II, we will proceed to discuss the methods for our models of Cu-Zr, MD simulations, and structural analysis. Section III characterizes the basic icosahedral ordering in our systems as they are cooled from the liquid phase to the glass phase. In section IV we mea-

sure the population and distribution of connections in the icosahedral network. Sections V, VI, and VII, respectively, presents weighted connectivities, introduces a static length scale, and details the chemical compositions of the icosahedral networks for $Cu_{50}Zr_{50}$ and $Cu_{64}Zr_{36}$.

II. MOLECULAR DYNAMICS SIMULATIONS AND VORONOI TESSELLATION

The MD simulations conducted in this study use a semi-empirical potential developed by Mendelev et al, which describes many-body interactions using the Finnis and Sinclair (FS) generalization of the embedded atom method (EAM)[51]. It was created, in part, by being fitted to x-ray diffraction data, liquid density, enthalpy of mixing data, and first-principles results. The potential was developed with an emphasis on describing both liquid and amorphous Cu-Zr alloys, and was shown to provide a very good description of the structures and some properties of the liquid and glass phases of $Cu_{64.5}Zr_{35.5}$. An earlier version of this potential[52] was also shown to produce reliable atomic structures for $Cu_{64.5}Zr_{35.5}$ MG when compared to atomic structures generated by the reverse Monte Carlo (RMC) method, which was constrained by independent x-ray diffraction data and *ab initio* MD simulation results[47]. The semi-empirical potential used in this paper accurately recreates the properties of pure Zirconium and is expected to yield reasonable structures for $Cu_{50}Zr_{50}$ as well. Accordingly, the structure factor data and Voronoi polyhedra distribution obtained for this composition are in good agreement with the published x-ray and Voronoi polyhedra data of M. Li *et al.*[47](not shown).

Canonical (NVT) systems of $Cu_{50}Zr_{50}$ and $Cu_{64}Zr_{36}$ were simulated using LAMMPS[53]. Each simulation consists of 2000 atoms contained in a box with periodic boundaries. The initial configuration of an alloy is generated randomly, and the alloy is allowed to melt and evolve for .25 ns at 1600K, using 5 fs time steps. The alloy is subsequently quenched to its target temperature at a rate of 10^{12} K/s, with the volume of the simulation box set to yield zero pressure for this temperature. Finally, the quenched alloy evolves for 1 ns at the target temperature, during which 78 snapshots of the atomic configuration are recorded. The target temperatures used range from 300 K to 1600 K in steps of 100 K. The process is repeated so that, ultimately, three simulations with independent initial configurations were carried out for each of the fourteen target temperatures. To check for system size effects, canonical systems with 10,000 atoms and a target temperature of 300 K were also simulated for both alloy compositions. The approximate values of the glass transition temperatures (T_g) for $Cu_{50}Zr_{50}$ and $Cu_{64}Zr_{36}$ were found to be 700 K and 800 K, respectively. A discussion of cooling rates and semi-empirical potentials is provided in section VIII.

An analogous NPT simulation ($P = 0$) of $Cu_{50}Zr_{50}$ with a target temperature of 400 K was conducted for the sake of comparison. The resulting average partial pair correlation functions (ppcs) were found to be statistically identical to those from the corresponding NVT simulations.

The atomic structures in the MD-generated alloys were characterized using Voronoi polyhedron-analysis for each atom[6,54,55]. Using a procedure similar to that of Hsu and Rahman, cluster vertices that were separated by distances less than seven orders of magnitude of the simulation box edge length were consolidated into one vertex[56].

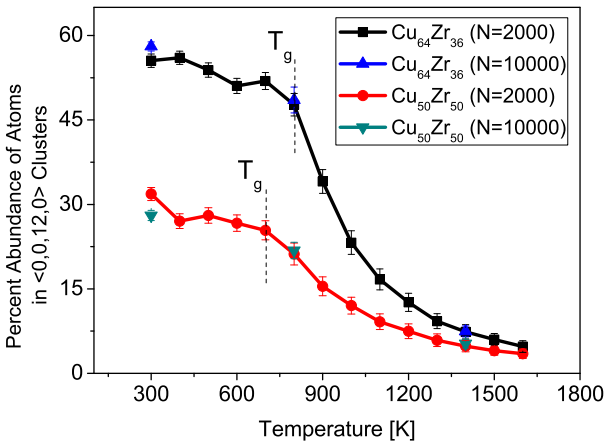

FIG. 1. (Color Online) Average percentage of atoms in a Cu-Zr alloy that participate in a 13-atom icosahedral cluster (center atom included). For T = 300 K, 800 K, and 1400 K, data points are included for a system size of $N = 10,000$ atoms in addition to $N = 2,000$ atoms. The error bars indicate the standard deviation of the value. The glass transition temperatures are marked for the respective compositions.

III. ICOSAHEDRAL ORDERING IN Cu-Zr ALLOYS

To study the development of icosahedral ordering in Cu-Zr, we consider the results of our Voronoi tessellation analysis: a Cu-atom with a Voronoi index $\langle 0,0,12,0\rangle$ and its 12 Voronoi neighbors form a full icosahedral cluster. The index $\langle n_3, n_4, ..., n_k, ...\rangle$ specifies the number of faces, n_k, with k edges present on the Voronoi polyhedron. Zr-centered full icosahedra are seldom observed amongst the Voronoi polyhedra in these alloys, which is consistent with previous MD studies, thus $\langle 0,0,12,0\rangle$ clusters will henceforth refer only to Cu-centered full icosahedra. Figure 1 displays for a range of temperatures the percent-abundance of atoms involved in $\langle 0,0,12,0\rangle$ clusters. In their liquid phases above 1300 K, fewer than 10% of the atoms participate in $\langle 0,0,12,0\rangle$ clusters for both compositions, but supercooling yields a great enhancement in the degree of icosahedral ordering. Accordingly, roughly 28% and 53% of the atoms of glassy $Cu_{50}Zr_{50}$

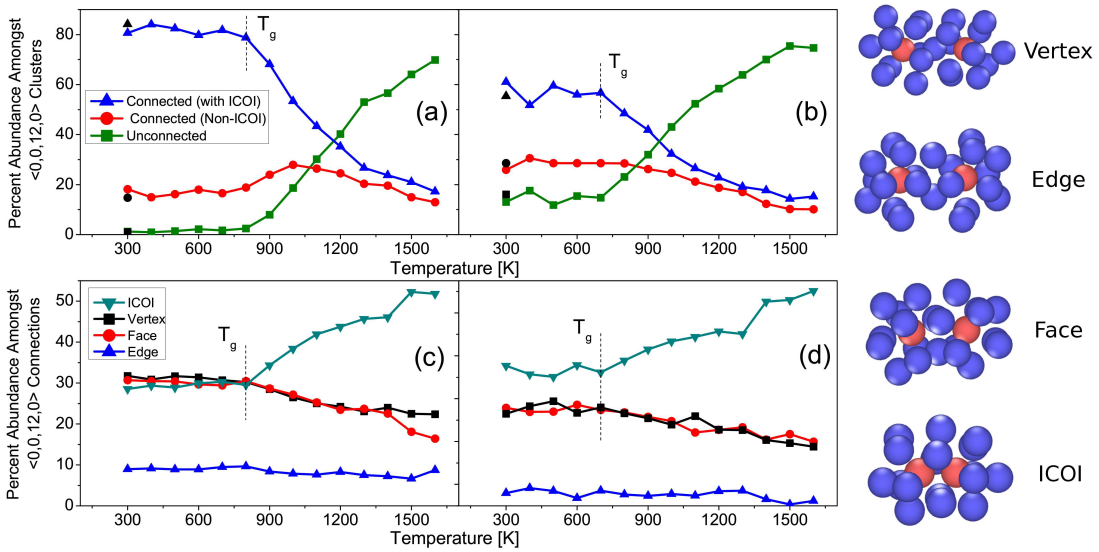

FIG. 2. (Color Online) [(a) and (b)] The average percentage of ⟨0,0,12,0⟩ clusters involved in: at least one ICOI connection, strictly non-ICOI connections, no connections for (a) $Cu_{64}Zr_{36}$ and (b) $Cu_{50}Zr_{50}$. The black symbols correspond to a system size of $N = 10,000$ atoms. [(c) and (d)] The average percent distribution of connection types between icosahedra in (c) $Cu_{64}Zr_{36}$ and (d) $Cu_{50}Zr_{50}$. The cluster snapshots in the right column of the figure depict the different types of connections between icosahedra. The red spheres represent the center Cu-atoms of the two icosahedra involed.

and $Cu_{64}Zr_{36}$, respectively, participate in the structure of full icosahedra (including their center Cu-atoms). This compositional trend of an increase in icosahedral ordering, and subsequently an increase in T_g, that accompanies an increase in the fractional abundance of Cu-atoms has been demonstrated and studied previously[40,41].

IV. ATOMIC CONNECTIONS BETWEEN ICOSAHEDRA

Below T_g, we observe that approximately 8.6% of $Cu_{64}Zr_{36}$'s Voronoi polyhedra in our simulation snapshots are ⟨0,0,12,0⟩ clusters. If these clusters were isolated from one another, it would require that 112% of the system's atoms participate in their structure. Considering that only about 53% of this alloy's atoms are actually involved in these clusters, it is obvious that many clusters share atoms amongst one another and are thus joined together. Therefore, two ⟨0,0,12,0⟩ clusters are defined to be 'connected' if they share at least one atom. The inclusiveness of this definition will be justified as we further study the details of icosahedral structures. Icosahedra in our simulated Cu-Zr alloys are observed sharing vertices, edges, and triangular faces in addition to exhibiting the interpenetrating connections described earlier. Examples of these connections are depicted in Figure 2. We will study the creation of these connections between icosahedra during the process of quenching to understand how they form the mechanically-stiff icosahedral networks.

Figure 2 quantifies the development of connections between icosahedra as the Cu-Zr alloys are quenched from the liquid phase. Figures 2a and 2b illustrate that as the number of icosahedra in a Cu-Zr alloy increases rapidly during supercooling (refer to Figure 1), the proportion of those participating in these stable ICOI grow comparably. Above 1300K, less than a third of the icosahedra are involved in ICOI for both alloys. The prevalence of ICOI-based structures is heightened dramatically during supercooling, and once $Cu_{64}Zr_{36}$ and $Cu_{50}Zr_{50}$ are arrested in their glass phases, approximately 80% and 60%, respectively, of icosahedra have at least one interpenetrating connection. Very few icosahedra are isolated in glassy Cu-Zr MGs, e.g, about 1.7% and 14%, respectively, in $Cu_{64}Zr_{36}$ (Fig. 2a) and $Cu_{50}Zr_{50}$ (Fig. 2b). Figures 2c and 2d display the relative abundance of each connection-type in the alloys. They show that vertex and face-sharing connections become increasingly prevalent as the alloys are quenched and enter their glass phases. For example, below T_g in $Cu_{64}Zr_{36}$, these connections are as common are ICOI (Fig. 2c). This is in stark contrast to the aforementioned results of Figures 2a and 2b, indicating that, as the density of icosahedral clusters and the number of ICOI increase during supercooling, vertex and face-sharing become prevalent amidst ICOI-based structures. We will further study how these non-interpenetrating connections are incorporated into the icosahedral structures of Cu-Zr MG alloys.

Above 1300 K, the connections between icosahedra are constantly forming and breaking (as are the icosahedra themselves) so that no single connection between two icosahedra is observed in consecutive snapshots (separated by 13 ps) of a simulation. Viewing snapshots of the liquid alloys and assessing the average abundances of

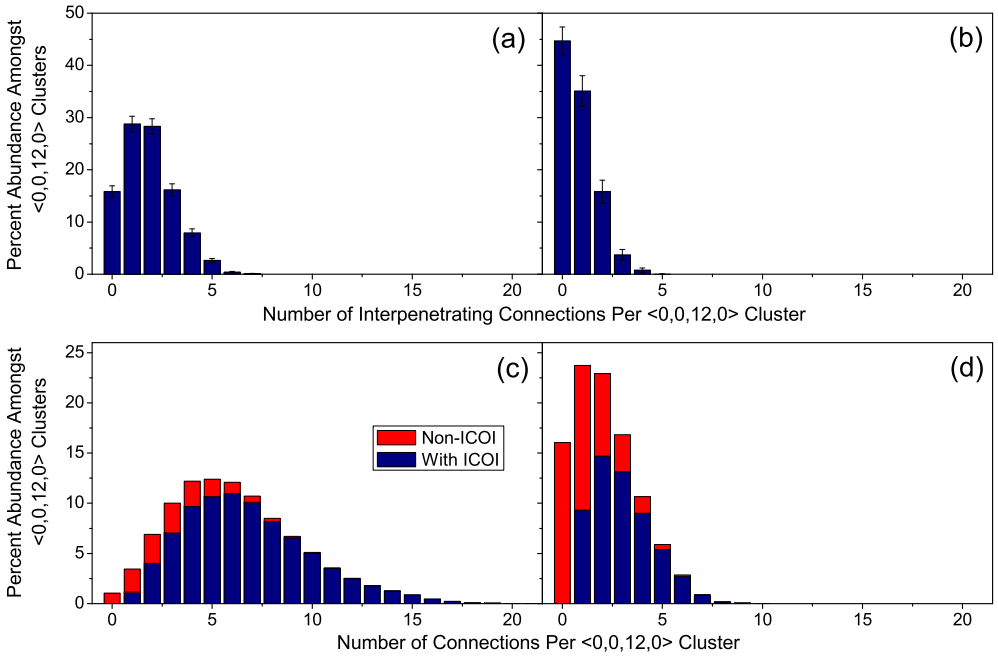

FIG. 3. (Color Online) [(a) and (b)] The average distribution of the number of interpenetrating connections per icosahedron in (a) $Cu_{64}Zr_{36}$ and (b) $Cu_{50}Zr_{50}$ MGs at 300 K ($N = 10,000$ atoms). The error bars indicate the estimated error in the mean value. [(c) and (d)] The average distribution of the number of connections (vertex, edge, face-sharing, or interpenetrating) per icosahedron in (c) $Cu_{64}Zr_{36}$ and (d) $Cu_{50}Zr_{50}$ MGs at 300 K ($N = 10,000$ atoms). These are stacked-histogram plots in which the blue bars correspond to icosahedra that participate in at least one interpenetrating connection, and the red bars correspond to those that do not participate in ICOI.

the different connection-types thus provides a measure of the relative prominences and stabilities of their resulting structures. Figures 2c and 2d show, for temperatures above 1000 K, that ICOI comprise more than 40%, a significant majority, of the connections present in both alloys. This provides strong evidence that the ICOI is in fact more robust than the other types of connections and leads us to consider its role in the liquid alloys as they cool. It is incorrect, however, to think of the glassy icosahedral network as simple chains of interpenetrating icosahedra, as our considerations of Figures 2c and 2d below T_g demonstrate that these ICOI structures also incorporate a significant number of non-interpenetrating connections, as we elaborate on next.

V. NON-INTERPENETRATING CONNECTIONS AND NETWORK CONNECTIVITY

To study the structures of the icosahedral networks found in Cu-Zr MGs, we begin by characterizing the formative ICOI-structures. Figures 3a and 3b show the average distribution of the number interpenetrating connections per icosahedron in the alloys at 300 K. As expected from our considerations of Figure 2, $Cu_{64}Zr_{36}$ contains more extensively connected ICOI-structures than does $Cu_{50}Zr_{50}$ MG with an average of 2.2 interpenetrations per connected-icosahedron versus 1.5, respectively. Both compositions primarily exhibit chain-like and triangular arrangements of interpenetrating icosahedra. These connectivity measurements are corroborated and elaborated on by earlier studies[42,47]. Figures 3c and 3d incorporate all connection types, and provide a uniquely detailed characterization of the icosahedral-structures found in these MGs. They display the average distribution of the total number of connections per icosahedron, while distinguishing icosahedra that participate in ICOI from those that do not. From this perspective, the average numbers of connections per interpenetrating icosahedron increase to 6.8 and 3.0, respectively, for $Cu_{64}Zr_{36}$ and $Cu_{50}Zr_{50}$. These distributions thus describe more intricate, highly connected networks than do to those in Figures 3a and 3b. Furthermore, it becomes clear that interpenetrating icosahedra frequently participate in other connection types and that they serve as the nodes with the highest connectivity in the icosahedral networks of the MGs. For example, in $Cu_{64}Zr_{36}$ a sizable fraction of ICOI-icosahedra can be found participating in ten or more connections, while non-ICOI-icosahedra are seldom found with more that six connections. It follows that significant number of non-interpenetrating connections must occur within and between ICOI-structures. These highly connected nodes in the networks likely correspond

to icosahedra with very low atomic mobilities, which are known to be responsible for dynamical slowing in these MGs[34,41,42]. When inspecting such densely packed icosahedra, simulation snapshots reveal two common structures, which are illustrated in Figure 4. Note that the black lines in this figure do not represent electronic bonding, rather, they indicate shared vertex atoms, between central Cu-atoms, that cannot be depicted without obscuring the snapshots. In 'pinned' structures (Figure 4a), a single extended ICOI-structure is folded on itself so that non-adjacent (non-interpenetrating) icosahedra can be found to share vertices, edges, and faces with one another, pinning the fold, and producing a densely packed, stable, extended structure. A 'bridged' structure (Figure 4b) consists of proximate ICOI-structures that are joined by non-interpenetrating connections. The roles of these bridging connections are of considerable interest since they serve to unify icosahedral networks and thus potentially affect the structure-property relationships of the MG. To demonstrate the significance of these bridging connections, we measured the weighted connectivities of the icosahedral networks.

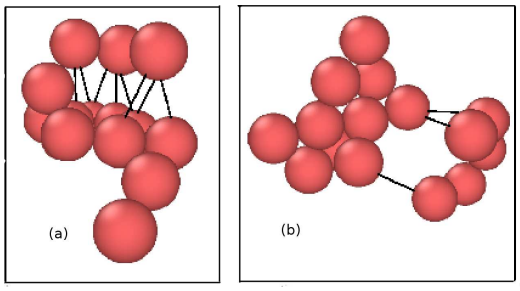

FIG. 4. (Color Online) Simulation snapshots[57] of icosahedral structures containing a) pinning and b) bridging connections. Only the central Cu atoms of the icosahedra are displayed. Black lines are drawn between center Cu atoms to indicate non-ICOI (vertex, edge, or face-sharing) connections between their respective icosahedra.

Consider the icosahedra of a Cu-Zr MG to be the nodes of a graph, G, and their connections as the edges. That is, if two icosahedra share a vertex, edge, or face, or if they interpenetrate, then there is an edge between these two nodes. A connected subgraph, V, of G is defined to be a collection of nodes and their edges such that any two nodes in V are joined by a path of edges and nodes, and that no edge connects to a node outside of V. The size of V is defined to be the number of nodes in V. In this paper, an isolated node (one without edges) will be considered a connected subgraph of size 1. Our graph, G, is thus the union of all of its connected subgraphs. Let $\{V_i\}_{i=1}^n$ be the set of G's n connected subgraphs and $\{S_i\}_{i=1}^n$ be the corresponding set of the sizes of the connected subgraphs. S_{max} is the size of the largest subgraph(s) ($S_{max} \equiv max(\{S_i\}_{i=1}^n)$). The weighted connectivity of G is then defined to be

$$W_G \equiv \sum_{k=1}^{n} \frac{S_k}{S_{max}} \tag{1}$$

Thus a graph with $W_G = 1$ corresponds to a completely connected graph. A heuristic example of a graph, its connected subgraphs, and its weighted connectivity is provided in Figure 6.

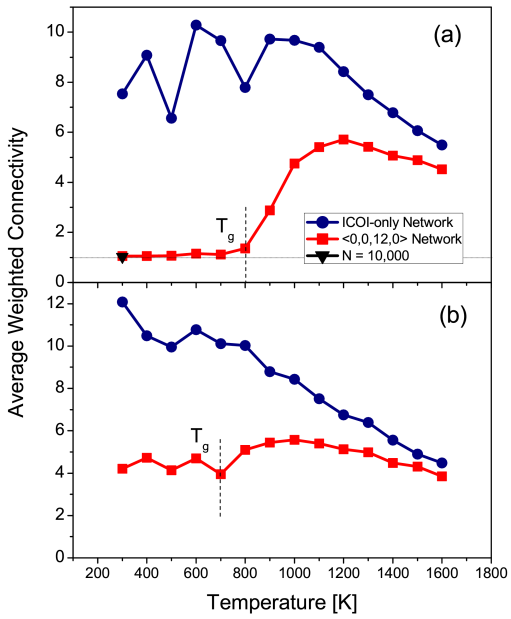

FIG. 5. (Color Online) The average weighted connectivity for the ICOI-icosahedral network (blue circles) and the full icosahedral network (red squares), which includes all connection types, for (a) $Cu_{64}Zr_{36}$ and (b) $Cu_{50}Zr_{50}$

Figures 5a and 5b show the weighted connectivities of both the ICOI-networks and the icosahedral networks that incorporate all connection types. It should immediately be pointed out that the decrease in weighted connectivity for high temperatures does not imply that the networks are highly connected prior to supercooling. Rather, the relatively low degree of icosahedral ordering at these temperatures is responsible for the reduced measured connectivities. In both compositions of Cu-Zr,

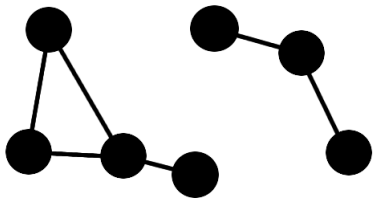

FIG. 6. An example graph, G, containing two connected subgraphs of sizes 4 and 3, respectively. The weighted connectivity of G is thus: $W_G = \frac{4}{4} + \frac{3}{4}$

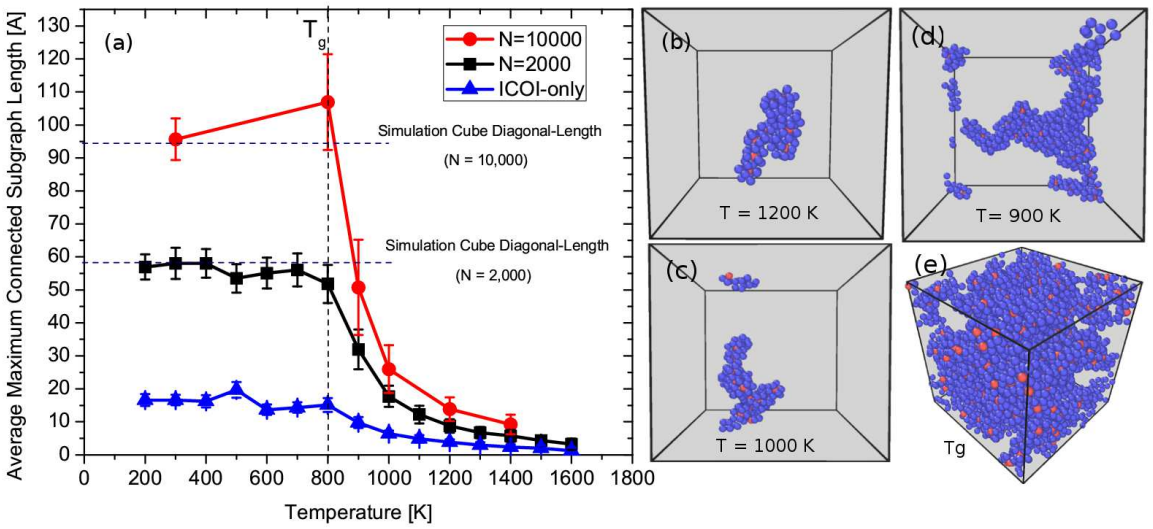

FIG. 7. (Color Online) (a) The average maximum icosahedron-to-icosahedron distance within a connected subgraph of the icosahedral network of $Cu_{64}Zr_{36}$. The simulation box employs periodic boundaries, thus seemingly disjoint atoms are attached to the connected subgraph across the box boundaries. As indicated, the horizontal dashed lines denote $\sqrt{3}l$, where l is the respective simulation cube side length. The blue triangles correspond to the longest connected subgraph lengths when only considering ICOI for forming edges of the graph. The error bars indicate the standard deviation in the maximum subgraph length. [(b) - (e)] Illustrative simulation snapshots[57] depicting the longest connected subgraph of the full icosahedral network at temperatures (b) 1200 K, (c) 1000 K, (d) 900 K, and (e) T_g (800 K). The red spheres depict center Cu atoms of $\langle 0,0,12,0\rangle$ clusters. The blue spheres depict both Cu and Zr atoms that serve strictly as vertices of the $\langle 0,0,12,0\rangle$ clusters. The perspective in (e) was changed in order to show the extent of the percolating subgraph.

the non-interpenetrating connections that develop during supercooling dramatically enhance the unification of the networks. The effect of these connections is most obvious in $Cu_{64}Zr_{36}$ MG (Fig. 5a); the weighted connectivity of the icosahedral network decreases rapidly as the alloy is cooled from 1100 K down to 800 K (T_g). In contrast to this, the weighted connectivity of the ICOI-network is not so significantly affected by the supercooling process. This suggests that non-interpenetrating connections are integral in linking the disjoint pieces of the ICOI-network as the alloy approaches its glass phase. In the case of $Cu_{64}Zr_{36}$, these bridging connections lead to an almost completely unified icosahedral network. The same network-unification was observed when the system size was increased to $N = 10,000$ atoms. The weighted connectivity of $Cu_{50}Zr_{50}$'s icosahedral network (Fig. 5b) exhibits a similar enhancement in comparison to its ICOI network, though network-unification is not observed in this alloy.

These findings suggest that non-interpenetrating connections are an important facet of icosahedral networking in Cu-Zr MGs and perhaps in other MGs in which icosahedral ordering is prevalent. The heavy presence of these connections amidst the most highly-connected icosahedra suggests that they may assist in the dynamical slowing of these clusters. It is also reasonable to expect that their roles in enhancing the density and structural unification of the icosahedral network's MRO-structures contribute significantly to the structural-mechanical properties that were previously attributed only to ICOI-structures[42,46]. Pins and bridges may be particularly important for compositions of Cu-Zr MG for which the development of ICOI is less extensive, and yet are good glass formers. As indicated earlier, only about 60% of the icosahedra in $Cu_{50}Zr_{50}$ MG participate in interpenetrating connections, but its icosahedral network is further developed via other connection types (Fig.3). We are also interested in studying whether the icosahedral network's weighted connectivity is simply related to the population density of icosahedra, or if approaching a completely unified network reveals more complex features.

VI. STATIC LENGTH SCALE

Quenching a supercooled liquid into a glass produces major changes in the system's dynamics, yet there is no obvious long range structural change that accompanies this transition. Despite this, rigorous bounds have been proven to exist between length and time scales in a glassy system which mandate that a growing length scale must accompany the diverging relaxation times of glass transitions[33]. Recent research efforts provide evidence for various growing correlation lengths[18,19,21–23,34]. However, there are findings that these scales (and in particular static length scales- i.e., those that can be ascertained from static snapshots of the system) do not increase, when approaching the glass transition, rapidly

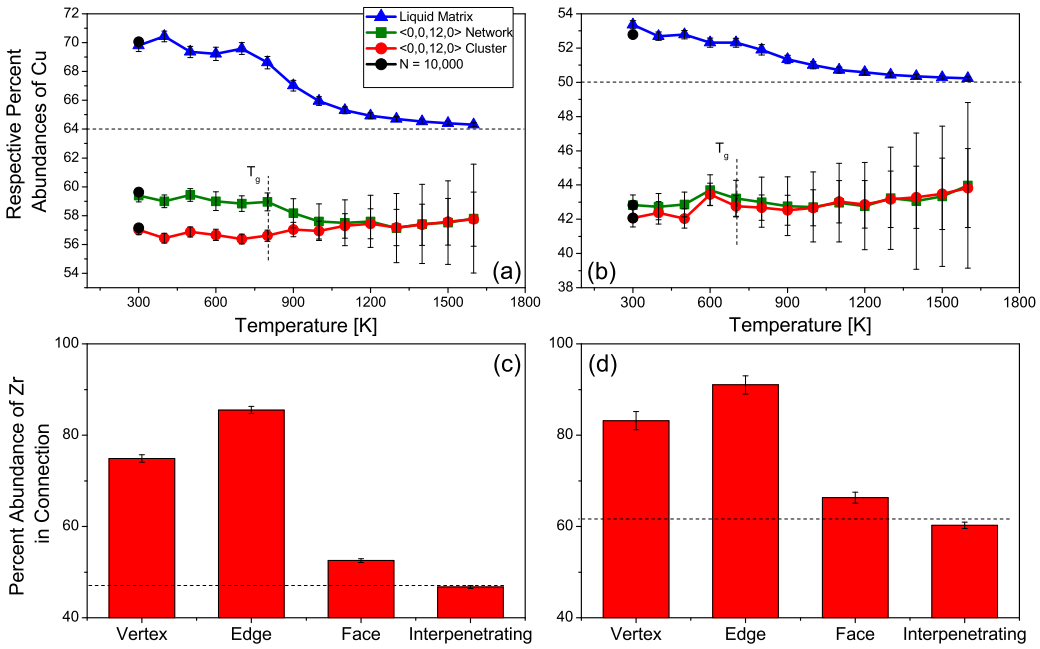

FIG. 8. (Color Online) [(a) and (b)] The average percent composition of Cu present in: a single icosahedral cluster (including the center atom), the full icosahedral network, the liquid-like matrix (all atoms not involved in the icosahedral network) for (a) $Cu_{64}Zr_{36}$ and (b) $Cu_{50}Zr_{50}$. [(c) and (d)] Display the average percent-abundance of Zr found in vertex, edge, face-sharing, and interpenetrating connections. The dotted lines indicate the percent-composition of the shell of an icosahedral cluster for (c) $Cu_{64}Zr_{36}$ and (d) $Cu_{50}Zr_{50}$. The error bars indicate the error in the mean values.

enough, as suggested by various theories , in order to account for the dramatic increase in the relaxation times[29]. Static correlation lengths have been studied via 'point-to-set' correlations[18,24,25], three-point correlations[26], pattern repetition size[27], and approaches employ graph theoretical tools[28] and shear rigidity penetration depths. Currently, most of the intuitive length scales, especially static ones, do not increase as drastically as does the relaxation time upon the glass transition. As glasses are rigid, a length characterizing the scale on which the supercooled liquid can support shear[28] may be anticipated to naturally increase as the system "freezes" into a rigid amorphous solid.

Motivated by these quests and, most notably, by the icosahedral network-unification that we observe in $Cu_{64}Zr_{36}$ during its glass transition, we introduce a static length scale, which interestingly exhibits dramatic growth upon quenching. Our length scale is the longest icosahedron-to-icosahedron distance within a connected subgraph of the full icosahedral network. It may be conceivable that the percolating icosahedral structure and the related increase in the interpenetrating icosahedral unit structure that we find might be related to an increased rigidity of the system as it rapidly cooled towards the low temperature glassy state. Connected subgraphs that cross the periodic boundaries are appropriately 'unfolded' across the boundaries before the distance is measured, and the maximum length is averaged across consecutive simulation snapshots. Figure 7 depicts the rapid growth in the length scale as $Cu_{64}Zr_{36}$ is cooled to T_g. From 1600 K down to T_g, the longest ICOI-chain length grows by a factor of 13. For the full icosahedral networks of the $N = 2,000$ atom and $N = 10,000$ atom systems, the longest connected subgraph lengths increase by factors of 19 and 31, respectively. As expected from the percolating nature of the network, and as indicated by the horizontal dashed lines in Fig. 7, the extent by which the length scale grows is apparently limited only by the simulation cell size.

VII. COMPOSITIONAL INHOMOGENEITY

Finally, we characterized the average chemical compositions of a single icosahedral cluster (including its center atom), the icosahedral network, and the different connection types. The results are summarized in Figure 8. The icosahedral networks of both Cu-Zr alloys were found to be Zr-rich relative to their overall system compositions. This leaves the remaining liquidlike matrix of the systems to be Cu-rich, as shown in Figures 8a and 8b. Figure 8c displays the average percent abundance of Zr in each type of connection. Comparing these ratios to the average icosahedral-shell composition (also displayed in Figure 8c) reveals that non-interpenetrating connec-

tions do not appear to occur randomly between icosahedra, rather, they preferentially incorporate Zr-atoms. Because Zr has a larger atomic volume than Cu, these connections increase the density of the icosahedral network, while preserving the local composition of a single icosahedral cluster.

VIII. CONCLUSION AND DISCUSSION

In summary, we used a semi-empirical potential to conduct MD simulations of $Cu_{50}Zr_{50}$ and $Cu_{64}Zr_{36}$ across liquid and glass-phase temperatures. Our initial assessment of icosahedral ordering and networking within these systems provides additional support for the popular idea that interpenetrating connections serve to create robust, formative icosahedral structures. Non-interpenetrating connections are shown, however, to become increasingly prevalent as the alloys approach their glass phases. Viewing icosahedra as members of a network, interpenetrating icosahedra frequently participate in non-interpenetrating connections as well, and distinctly serve as the nodes of the network with the most connections. In particular, non-interpenetrating 'pinning' and 'bridging' connections are prominent amongst ICOI-structures, and may be of particular structural importance in Cu-Zr MGs in which ICOI are less extensive. To further characterize the structure of the icosahedral networks, we introduced the measure of weighted connectivity and used it to show that the network of $Cu_{64}Zr_{36}$ is almost completely unified, in contrast to its ICOI-structures. Accordingly, the maximum connected-cluster length lends itself as a static length scale, whose rapid growth upon quenching is apparently limited only by the simulation cube size. Lastly, the vertex, edge, and face-sharing connections are shown to preferentially incorporate Zr atoms, amidst icosahedral networks that are Zr-rich compared to the system compositions.

It is important for the reader to note that the relaxation times involved in this and in all concurrent classical MD studies of glasses are restricted such that experimental cooling rates are several orders of magnitude slower in reality[9,47]. To this end, the effects of fast cooling rates were assessed in the appendix of the work by M. Li *et al.*[47], which demonstrated that the partial pair correlation functions, the statistical distribution of Voronoi polyhedra, and the spatial correlations between Voronoi polyhedra are all robust in $Cu_{64.5}Zr_{35.5}$ across two orders of magnitude of cooling rates and between classical MD results and *ab initio* simulation results. Furthermore, they found that the formation of the stringlike ICOI-network is facilitated by slower cooling rates, hinting that real glasses would exhibit an even more highly connected icosahedral network.

The semi-empirical potential used in a classical MD simulation obviously affects, fundamentally, the structural and dynamical features exhibited by a system[9]. To this end, the dynamics of viscous slowing in a liquid can depend nontrivially and nonperturbatively on the form of the potential, while the static structure of the system is less sensitive[58]. The present study only focuses on structure of Cu-Zr MGs, the features of which are largely reproduced by a number of independently developed Cu-Zr semi-empirical potentials[34,41,42,47] and by *ab initio* studies.[47,59]

IX. ACKNOWLEDGMENTS

We thank Nick Mauro, and James Bendert for their useful discussions. R.S. and L.Y. were partially supported by the National Science Fundation (NSF) Grant No. DMR-1207141. Z.N. was partially supported by NSF Grant No. DMR-1106293. K.F.K was partially supported by NSF under grants DMR-08-56199 and DMR-12-06707, and NASA under grants NNX07AK27G and NNX10AU19G.

[1] A.L. Greer and E. Ma, MRS Bulletin **32**, 611 (2007).
[2] K.F. Kelton *et al.*, Physical Review Letters **90**, 195504 (2003).
[3] Hans Sillescu, Journal of Non-Crystalline Solids **243**, 81-108 (1999).
[4] G.A. Appignanesi *et al.*, Physical Review Letters **96**, 237803 (2006).
[5] L. Berthier and R. Jack, Physical Review E **76**, 041509 (2007).
[6] Y.Q. Cheng and E. Ma, Progress in Materials Science **56**, 379-473 (2011).
[7] D. Miracle, Nature Materials **3**, 697-702 (2004).
[8] H.W. Sheng *et al.*, Nature **439**, 419-425 (2006).
[9] L. Berthier and G. Biroli, Rev. Mod. Phys. **83**, 587-639 (2011).
[10] V. Lubchenko and P.G. Wolynes, Rev. Phys. Chem. **58**, 235-266 (2007).
[11] T.R. Kirkpatrick *et al.*, Physical Review A **40**, 1045-1054 (1989).
[12] M.Tarzia and M.A. Moore, Physical Review E **75**, 031502 (2007).
[13] W. Gotze, J. Phys.: Condensed Matter **11**, A1 (1999).
[14] P. Mayer *et al.*, Physical Review Letters **97**, 095702 (2006).
[15] J.P. Garrahan. J. Phys.: Condensed Matter, **14**, 1571-1579 (2004).
[16] Z. Nussinov, Physical Review B. **69**, 014208 (2004).
[17] G.Tarjus *et al.*, J. Phys.: Condensed Matter **17**, R1143-R1182 (2005).
[18] G. M. Hocky *et al.*, Physical Review Letters **108**, 225506 (2012).
[19] H. Tanaka *et al.*, Nature Materials **9**, 324 (2010).

[20] S. Karmakar *et al.*, PNAS **106**, 3675 (2009).
[21] M. Mosayebi *et al.*, Physical Review Letters **104**, 205704 (2010).
[22] L. Berthier *et al.*, Science **310**, 1797 (2005).
[23] S. Karmakar *et al.*, Proc. Natl. Acad. Sci. U.S.A **10**, 3675 (2010).
[24] G. Biroli *et al.*, Nature Phys. **4**, 771 (2008).
[25] J.P. Bouchaud and G. Biroli, J. Chem. Phys. **121**, 7347 (2004).
[26] D. Coslovich, arXiv:1212.5360 (2012).
[27] J. Kurchan and D. Levine, e-print arXiv:094.485 (2009).
[28] P. Ronhovde *et al.*, European Physics Journal E **34**, 105 (2011); P. Ronhovde *et al.*, Scientific Reports **2**, 329 (2012).
[29] P. Charbonneau and G. Tarjus, arXiv:1211.4821v1 [cond-mat.dis-nn] (2012).
[30] F. Ritort and R. Moserri, Adv. Phys. **52**, 219-342 (2003).
[31] E. Aharanov *et al.*, Euro. Phys. Lett. **77**, 56002 (2007).
[32] D. Chandler and J.P. Garrahan, Annu. Rev. Phys. Chem. **61**, 191-217 (2010).
[33] A. Montanari and G Semerjian, J. Stat. Phys **125**, 23 (2006).
[34] K.N. Lad **et al**., The Journal of Chemical Physics **136**, 104509 (2012).
[35] M.B. Tang *et al.*, Chin. Phys. Lett. **21**, 901 (2004).
[36] P. Yu *et al.*, Journal of Non-Crystalline Solids **351**, 1328-1332 (2005).
[37] O.J. Kwon *et al.*, Metals and Materials International **12**, 207-212 (2006).
[38] Y.Li *et al.*, Science **322**, 1816 (2008).
[39] J.C. Bendert *et al.*, Phys. Rev. Letters **109**, 185901 (2012).
[40] N. Mattern *et al.*, Journal of Non-Crystalline Solids **354**, 1054-1060 (2008).
[41] Y.Q. Cheng *et al.*, Physical Review B **78**, 014207 (2008).
[42] M. Lee *et al.*, Acta Materialia **59**, 159-170 (2011).
[43] T. Schenk *et al.*, Physical Review Letters **89**, 075507 (2002).
[44] Y.Q. Cheng, A.J. Cao, and E. Ma, Acta Materialia **57**, 3253-3267 (2009).
[45] D. Nelson, Physical Review B **28**, 5515 (1983).
[46] M. Wakeda and Y. Shibutani, Acta Materialia **58**, 3963-3969 (2010).
[47] M. Li *et al.*, Physical Review B **80**, 184201 (2009).
[48] T. Tomida and T. Egami, Physical Review B **52**, 3290(19) (1995).
[49] M. Shimono and H. Onodera, Materials Science Forum Vols, 2031-2035 (2007).
[50] A. Takeuchi and A. Inoue, Materials Transactions **53**, 1113-1118 (2012).
[51] M.I. Mendelev *et al.*, Philosophical Magazine **89**, 967-987 (2009).
[52] M.I. Mendelev *et al.*, Journal of Applied Physics **102**, 043501 (2007).
[53] S. Plimpton, Journal of Computational Physics **117**, 1-19 (1995). http://lammps.sandia.gov
[54] J.L. Finney, Proceedings of the Royal Society of London: Series A, Mathematical and Physica; Sciences **319.1539**, 479-493 (1970).
[55] G. Voronoi, Journal für die Reine und Angewandte Mathematik, **134** 198-287 (1908).
[56] C.S. Hsu and A. Rahman, Journal of Chemical Physics, **71.12** 4974-4986 (1979).
[57] A. Stukowski, Modelling and Simulation in Materials Science and Engineering, **18** 015012 (2010). http://ovito.org/
[58] L. Berthier and G. Tarjus, Physical Review Letters, **103** 170601 (2009)
[59] N. Jakse and A. Pasturel, Physical Review B, **78** 214204 (2008)